Proceedings of 8th International Conference on Mechanical, Industrial and Energy Engineering 2024
02-04 January, 2025, Khulna, BANGLADESH
SciEn Conference Series: Engineering Vol. 3, 2025, pp 701-706 https://doi.org/10.38032/scse.2025.3.176

Effect of Corrugation on the Stall Angle Characteristics of NACA 0012 Airfoil: A Numerical Approach

Fahim Al Galib, Adnan Roshid Shawon, Mohammad Ilias Inam*

Department of Mechanical Engineering, Khulna University of Engineering & Technology, Khulna-9203, Bangladesh

ABSTRACT
The aim of the study is to numerically examine the effect of corrugation on the stall angle characteristics including the coefficient of lift and drag NACA 0012 airfoil. The FLUENT module of ANSYS version 2020 R1 software was employed for performing the simulations to compute the lift coefficient and drag coefficient at various incidence angle (α) and a Reynolds number (Re) of definite value 2.5×10^5. A sinusoidal corrugation profile was inserted at the apt 1/3rd of the chord on the upper surface. The numerical results indicate that the corrugation delays the flow separation improving the stall characteristics whereas some penalty on other aerodynamic characteristics was also noticeable such as lower value of lift coefficient at low angle of attack, higher drag coefficient compared to smooth airfoil. The stall angle is delayed by 3° and the maximum lift coefficient value significantly increased. Hence corrugation can be implemented to enhance some particular characteristics while sacrificing one or more other aerodynamic performances. The optimization of the profile is required to achieve the desired improvement and minimize the adverse effects.

Keywords: Corrugated Airfoil, Stall Angle, Flow Separation, ANSYS FLUENT.

1. Introduction

Inspired by natural flyers like dragonflies, corrugated airfoils have drawn attention because of their distinctive aerodynamic qualities, especially at low Reynolds numbers. Under some circumstances, the wavy, corrugated surface of these airfoils can improve aerodynamic performance. Corrugated skins can be a good alternative option for morphing wings because of their high anisotropy. If the low stiffness corrugation plane is oriented chordwise, the airfoil may undergo a form shift. Unlike the typical smooth airfoil, a corrugated skin has an influence on the local and global aerodynamics of a wing [1]. The expansion of the flying envelope and enhanced mission profile capabilities are two additional advantages that are typically associated with morphing aircraft. There has been a great deal of research on morphing concepts over the last two decades, with several studies taking into account modifications to the interior wing structure [2,3].

It is well acknowledged that the non-smooth surface operating at a high Reynolds (Re) number is inappropriate for an aerodynamic profile due to its relatively poor aerodynamic performance, which results in low lift and high drag. However, many insects, like as dragonflies and damselflies, have corrugated wing profiles that operate at relatively low Reynolds numbers [4]. At low Reynolds numbers, these wings enable them to have rigid, thin, and aerodynamically efficient wings i.e. 10^3 to 10^4 [5]. Both Okamoto et al and Tamai et al have experimented on insect wings and found better aerodynamic performance (e.g. lift-curve-slope, maximum lift-coefficient, minimum drag-coefficient, higher stall angle) than a flat plate at low angles of attack and low Reynolds numbers [5,6].

Some studies are focused on the impact of corrugated skins in the chord's aft 30% since they allow for significant variations in the surface area and airfoil camber along the chord (Thill et al., 2007; Yokozeki et al., 2006; Thill et al., 2008) [7-9]. Whitehead et al. (1982) and Thill et al. (2010) carried out wind tunnel experiments and numerical analysis of airfoils with corrugation in the aft one-third section of the chord at Reynolds numbers between 250,000 and 1,000,000 [10,11]. Hu, Tamai, Murphy, and Hu experimented corrugated aerofoils that demonstrated favorable aerodynamic performance and had cross sections similar to those of typical dragonfly wings. They found that flow-separation vortices trapped in the corrugation valleys pull fluid toward the aerofoil wall region, reducing the overall extent of the flow-separation zone. Lift-to-drag ratios can grow up to a chord Reynolds number of Re=125,000 as a result of these unique flow properties, which allow flow separations for these corrugated aerofoils to be delayed until a higher angle of attack [12,13]. However, there were significantly fewer corrugations in the corrugated aerofoil that Levy and Seifert investigated. Rather, their aerofoil featured a convex trailing-edge "hump" and a "saddle" after just two corrugations at the leading edge. In this instance, fewer flow-separation events propagate over the trailing edge because flow separations resulting from the upstream corrugations regularly reattach back to the trailing edge hump. Specifically, a recirculating vortex is seen to develop at the saddle, which is believed to be crucial in regulating flow separation [14].

T. H. New (2014) discovered that corrugations that are compacted in a small area with a huge peak have superior control over flow separation in his work on particle-streak visualizations and vorticity fields on NACA 0010 airfoils. By keeping the airflow affixed to the wing's surface, a large-

*Corresponding Author Email Address: ffahimalgalib@gmail.com

scale recirculating zone at a particular spot helps minimize the size of the flow-separation bubbles. In comparison to the typical NACA 0010 wing, the study reveals that the corrugated wings can considerably affect the air flow across the wing, reducing the magnitude of vortices and flow separations [15]. However, Shabbir's (2020) study, which used numerical analysis to examine the impact of corrugation peak shape, produced results that contradicted the circular corrugation findings over NACA airfoil. The paper states that lift is increased at low angles of attack when the corrugation peak is high. However, he also pointed out that a high angle of attack could cause a vortex to spill over, which would result in a high drag coefficient [16].

Thill et al. (2010) found in his experiment large amplitude corrugations typically result in a higher drag coefficient. This is because the thicker airfoil caused by the corrugations reduces drag by increasing resistance (pressure) over the airfoil. The drag coefficient was raised by fixed lift coefficients (the force required to maintain the airfoil in the air) and higher Reynolds numbers (faster air or larger airfoils). Airfoils with corrugations had more drag than smooth ones for the same lift. With six corrugations and a 1.0% amplitude, the greatest increase in drag was noted. According to the study, by lessening the pressure differential between the top and bottom surfaces, these corrugations lessen the wing's capacity to produce lift. This is because the airflow is disrupted by the uneven surface, making it more difficult for the wing to trap the air and create lift [11].

The objective of the present work is to investigate the effect of sinusoidal corrugation on the stall angle characteristics of the airfoil. The earlier work incorporated corrugation on both top and bottom surface of the airfoil which resulted in significant increase in drag coefficient. Moreover the previous works regarding corrugation mostly carried out for low and ultra-low Reynolds Number. A little concentration was given at high Re. Although the work done by Thill (2010) was at high Re, it mainly focused on the drag characteristics and lift-curve slope of the airfoil. But the impact on the stall angle and aerodynamic efficiency at high Re has not been explored. The current study aims to investigate the effect of top surface corrugation on those parameters at high Re value of 2.5×10^5.

2. Numerical Methods

2.1 Airfoil

For the current study, NACA 0012 aerofoil with sinusoidal corrugation of amplitude 4%c and wavelength 6.5%c placed at 30% apt of the chord was chosen to perform numerical analysis, the sketch is indicated by **Fig. 1**. According to its specifications, the NACA 0012 airfoil is symmetrical and has a maximum chord thickness of 12%. In this study, the length of the chord was taken 100 mm. Airfoil geometry was modeled on SOLIDWORKS by inserting the NACA 0012 coordinates file.

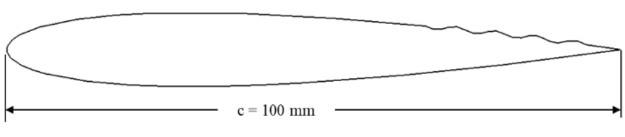

Fig.1 Profile shape of corrugated NACA 0012 aerofoil**.**

2.2 Numerical Methods

The simulations were carried out in Fluent module of ANSYS software. The solution of the problem was considered in steady-state condition. The Reynolds number was fixed for these simulations and was performed at Re equal to 2×10^5. The properties of air were considered constant and taken as follows: ρ = 1.225 kg/m^3, and μ = 1.7894 × 10^{-5} kg/ms [17]. For the solution of RANS (Reynolds Averaged Navier-Stokes) problem in steady state the gradient option based on Green-Gauss cells was employed. For the flow is considered incompressible the pressure-based solver was chosen. The time-averaged motion equations for fluid flow are known as the RANS equations are mentioned below:

$$\frac{\partial}{\partial x_i}(\rho u_i)= 0 \tag{1}$$

$$\frac{\partial}{\partial x_j}(\rho u_i u_j) = \frac{\partial p}{\partial x_i} + \frac{\partial}{\partial x_j}\left[\mu\left(\frac{\partial u_i}{\partial x_j} + \frac{\partial u_j}{\partial x_i} - \frac{2}{3}\partial_{ij}\frac{\partial u_l}{\partial x_l}\right)\right] + \frac{\partial}{\partial x_j}(-\rho\overline{u_i' u_j'}) \tag{2}$$

here density is represented by ρ, velocity by u, and fluid dynamic viscosity by μ. The average momentum variation of the fluid element resulting from instability of stream and convection by the mean fluid-flow is shown on the left side of this equation. The average body force, the viscous stresses, the isotropic stress from the average pressure field, and the visible stress from the varying velocity field all control this adjustment, usually known as the Reynolds stress $(-\rho\overline{u_i' u_j'})$. It is a nonlinear equation of stress which needs further modeling for resolving the RANS equations that may have different turbulence models [18].

2.2.1 SST k-ω Turbulence Modeling

For computational investigation SST (Shear Stress Transport) k - ω is extensively utilized two-equation turbulence model which integrates the benefits of the k-ε and k-ω models. It offers a universal solution for the specific dissipation rate of eddy viscosity (ω) and the turbulence kinetic energy (k). The following transport equations yield the turbulent kinetic energy k and the eddy viscosity dissipation rate ω (3) and (4):

$$\frac{\partial}{\partial x_i}(\rho k u_i) = \frac{\partial}{\partial x_j}\left[(\mu + \sigma_k\mu_t)\frac{\partial k}{\partial x_j}\right] + G_k - Y_k + S_k \tag{3}$$

$$\frac{\partial}{\partial x_i}(\rho \omega u_i) = \frac{\partial}{\partial x_j}\left[(\mu + \sigma_\omega\mu_t)\frac{\partial \omega}{\partial x_j}\right] + G_\omega - Y_\omega + S_\omega \tag{4}$$

where,

G_k= production of turbulent kinetic energy due to the mean velocity gradients

G_ω = Generation of ω

Y_k, Y_ω = Dissipation rate of turbulent kinetic energy (k) and ω

σ_k, σ_ω= Turbulent Prandtl number for k and ω

S_k, S_ω = Source terms or external factors affecting k and ω

The turbulence viscosity $\mu_t = \frac{\rho k}{\omega}\frac{1}{\max\left[\frac{1}{\alpha^*},\frac{SF_2}{\alpha_1\omega}\right]}$; here S indicates the magnitude of the rate of strain, F_2 is a constant, and α = Incidence angle.

2.3 Boundary Conditions

A computational regime was established surrounding the aerofoil to carry out the CFD analysis, as seen in **Fig. 1**. In order to reduce the viscous layer consequence the domain was enlarged 12.5%c ahead the upstream and 20%c towards downstream from the trailing edge, as shown in **Fig. 2** [19]. The airfoil surface was taken to be a no-slip boundary condition in the domain, the continuous line BAFED was considered as constant velocity inlet and pressure outlet is indicated by BCD. The entry velocity u was taken 36.5 m/s for the fixed value of Re. Rather than rotating the airfoil, the simulation altered the angles of attack (α) by altering the course of flow which provided the similar result. The x and y component of the velocity was determined for varying AoA.

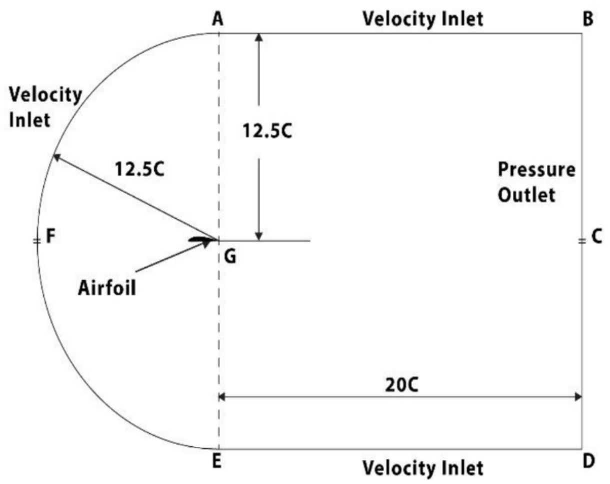

Fig.2 Computational zone with boundary conditions

2.4 Meshing

The mesh, structured mesh of C-type, was developed to improve wall function control and convergence, as seen in **Fig.3** and **Fig.4**. **Fig.3** illustrates the structured mesh having quadrilateral elements, created by ANSYS fluent mesh module while **Fig.4** demonstrate the mesh characteristic over the aerofoil surface having triangular elements.

While maintaining a satisfactory level of solution, the use of wall functions close to the airfoil surface may greatly lower the processing and storage needs. To make sure enough boundary layers modeled the inflation was set to 5.97 mm with 10 layers.

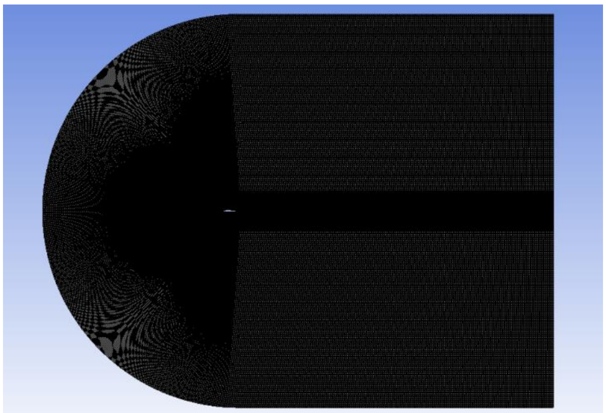

Fig. 3 Computational grid over the entire domain.

The effectiveness of $k - \omega$ model is about $y^+ \approx 1$. The non-dimensional wall parameter is defined as:

$$y^+ = \frac{\rho u_\tau y}{\mu} \quad (5)$$

Here y is the distance from the wall to the centroid of the first fluid cell.

The frictional velocity: $u_\tau = \sqrt{\frac{\tau_w}{\rho}}$ (6)

The value of y+ was found to be smaller than 1 for every simulation.

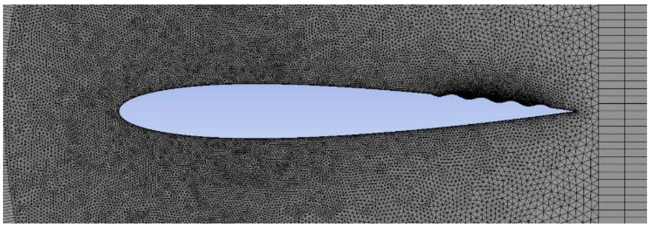

Fig. 4 Mesh around corrugated airfoil

2.5 Mesh Independence Test

To test grid independence, a number of simulations were performed. By changing the size of element of the circular and rectangular portion, different meshes were produced. The drag coefficient fluctuation for varying mesh element number at a 0° angle of attack is shown in Fig. 5. The figure shows that meshes with more than 350000 pieces can yield precise results with little variation. Meshes with element number 350000 were thus chosen for additional computation.

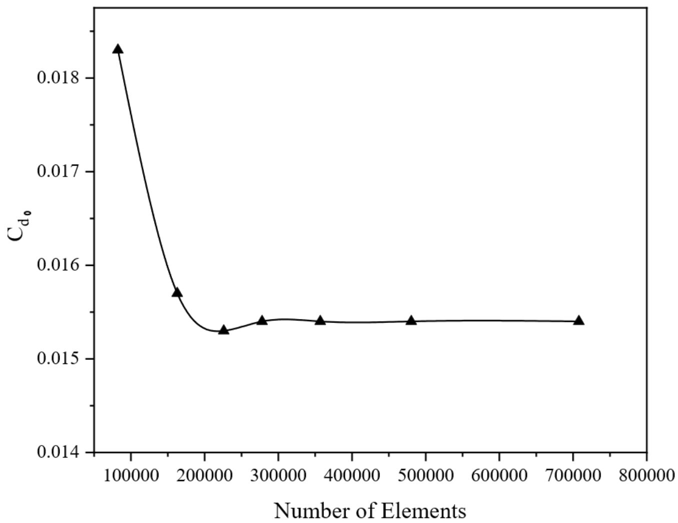

Fig.5 Change of drag coefficient with no. of elements.

3. Validation

The computational result was validated with the experimental work of Thill et al. (2010) who performed wind tunnel test for various corrugated shape of airfoil. A corrugation shape of wavelength 2.5%c and amplitude 0.6%c was selected for validation purpose. The value of obtained from computational method was in reasonable accuracy with the experimental one.

Table 1 Drag coefficient of the NACA 0012 airfoil with wavelength 2.5%c and amplitude of 0.6% of chord length at AoA 0°

Parameter	Experimental (Thill et al., 2010)	CFD	% Error
C_{d0}	0.0155	0.0154	0.645

4. Results and discussions

The lift coefficient fluctuation at various angles of attack is shown in **Fig. 6** for both conventional and corrugated NACA 0012 airfoil. It can be seen that corrugation profile has delayed the flow separation increasing the stall angle. For the conventional airfoil the flow separates around 11° angle of attack whereas for corrugated airfoil the stall occurs at 14°.

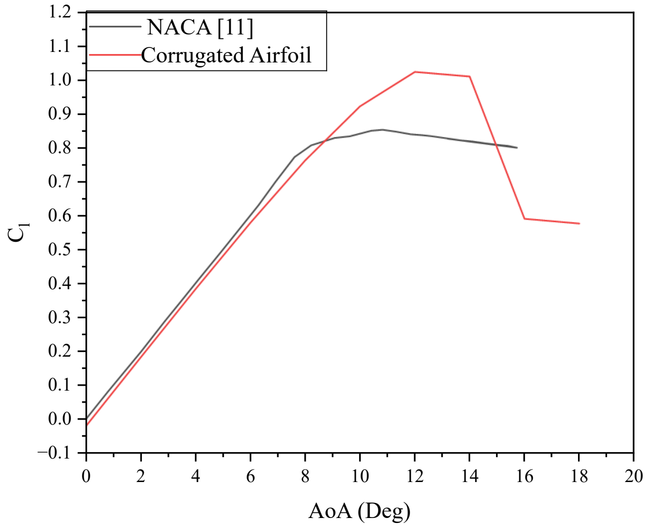

Fig.6 Lift coefficient of smooth and corrugated NACA 0012 airfoil at different AoA.

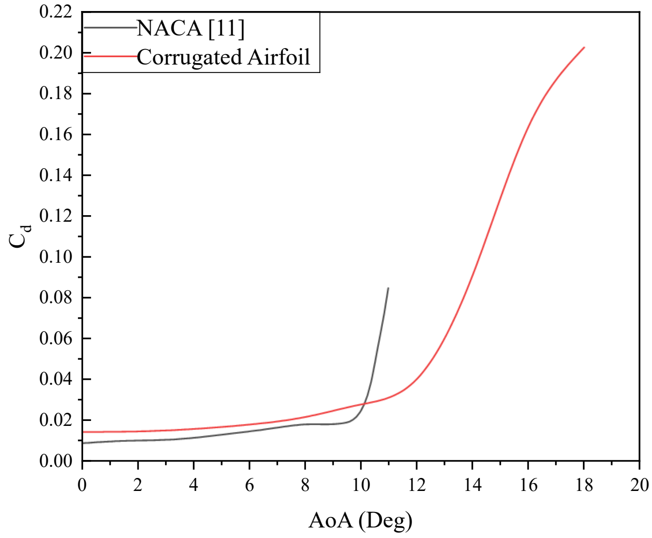

Fig.7 Drag coefficient of smooth and corrugated NACA 0012 airfoil at different AoA.

The reason is the corrugation profile keeps the flow relatively attached even at higher angle of attack. The flow separation primarily occurs due adverse pressure gradient along the flow direction. This positive pressure gradient causes the fluid to slow down and prevents them from entering into the foremost high pressure region. Consequently, the boundary layer gets separated. However, in case of corrugated surface the flow passes through the wavy path which results in negative pressure gradient. At the peak the gradient may be zero and tries to be positive further downstream. But the valleys of the profile traps the flow vortices inside them keeping it bounded to the airfoil surface which prevents flow separation. For both airfoil the lift coefficient increases with AoA. The lift curve slope is nearly the same for both airfoil up to 7° angle of attack. Also at smaller angle of attack the smooth profile produces a slightly higher lift coefficient. But at higher value of AoA the lift co-efficient of corrugated airfoil varies greatly and assumes a greater value than the conventional one. The possible reason of such phenomenon is the increase in the negative pressure at the upper surface of the aerofoil. At higher AoA the flow vortices in the corrugated valleys produces large negative pressure (**Fig.11**) that contributes to the increased lift coefficient. However, there is no mathematically defined relation of such manner. Moreover, the geometric factor also needs to be considered.

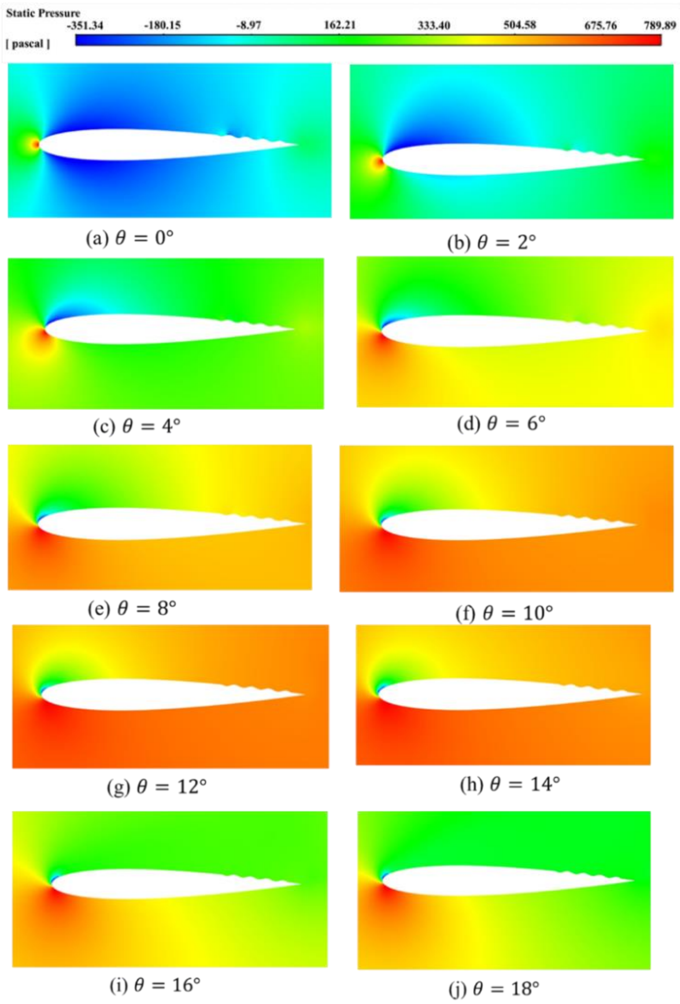

Fig.8 Pressure contours over airfoil surface at different AoA.

It is observed that at 0° AoA the lift coefficient assumes a negative value, the reason of which is not well understood. However, the maximum lift coefficient is much higher for corrugated airfoil. For the corrugated airfoil the maximum lift increased by 19.63% compared to smooth one. **Fig.7** illustrates the variation of drag coefficient with angle of attack. The corrugated surface adversely impact the drag coefficient. The non smoothness of the surface increases the resistance to flow which results in a higher drag coefficient.

Fig.8 represents the static pressure distributions over the airfoil surface of corrugated airfoil at different AoA. It can be seen that except for 0° angle the pressure is lower at the upper surface and higher at lower surface. The negative pressure region typically occurs at the upper surface which decreases with increase in angle of attack. This imbalance in pressure produces the net upward lift. Until the flow separation occurs, the pressure differential between the top and bottom surfaces increases. However, at zero degree AoA the case is different as the pressure assumes higher value at the upper surface than the lower one producing negative lift coefficient.

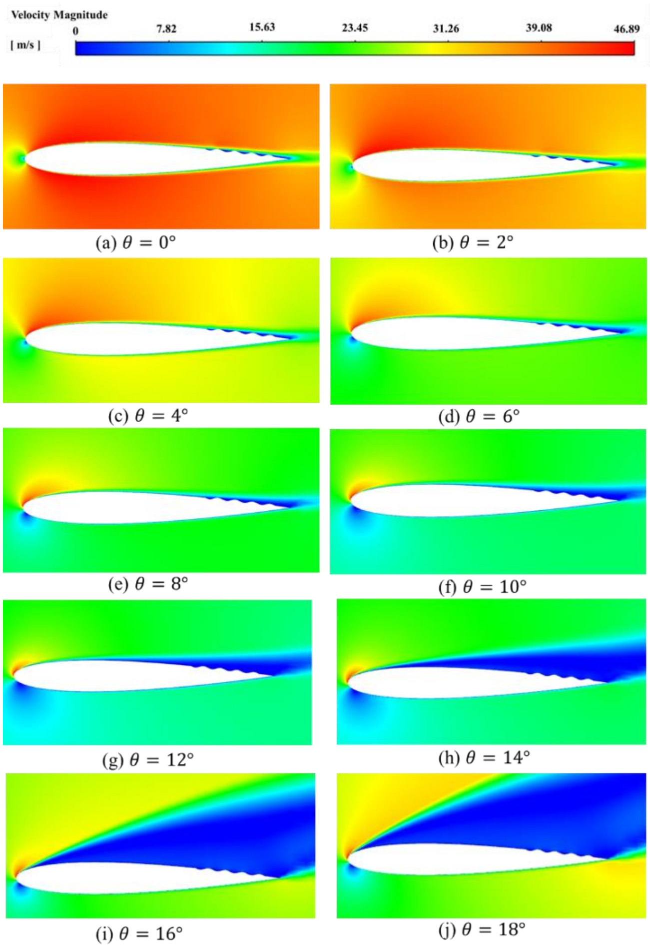

Fig.9 Velocity contour over airfoil surface at different AoA.

Fig.9 presents the variation of velocity magnitude at different angle of attack. It is evident that the velocity is higher at upper surface than lower surface. This is due to the squashing of air flow at the nose region of the of the upper surface which can be explained by Bournollie's principle. The flow stays connected to the top and lower surfaces at a reduced angle of attack. The flow starts to split at the trailing edge when the angle of attack reaches 8° and with increasing AoA it moves towards the leading edge.

Fig.10 shows the lift-to-drag ratio at different AoA for both the smooth and corrugated airfoil. This non-dimensional parameter represents the efficiency of the airfoil. It is clear from the graph that the corrugated surface reduces the efficiency of the airfoil. The greatest reduction is 29.5% which occurs at 4° angle of attack. The maximum value of lift to drag ratio is 44.06 and 35.16 for conventional and corrugated airfoil respectively. However, for both airfoil the maximum value occurs at 8° angle of attack. Furthermore at 10° AoA the value becomes nearly equal for both airfoil.

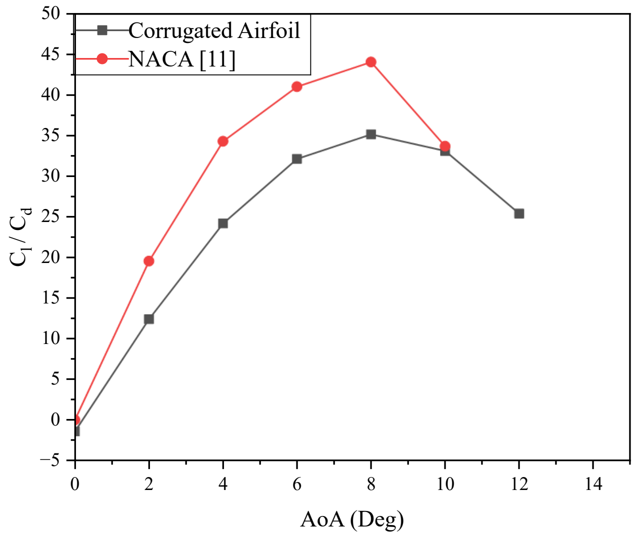

Fig.10 Lift-to-drag ratio at different AoA.

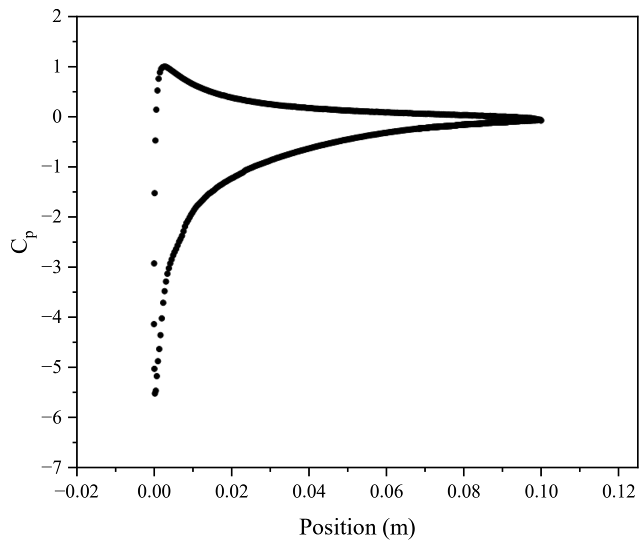

Fig.11 Pressure coefficient over the surface of corrugated airfoil at 12° AoA.

5. Conclusion

In this paper the influence of sinusoidal corrugation profile on the stall angle features of NACA 0012 airfoil have been studied using ANSYS FLUENT with SST k-ω turbulence model. The effects were compared with that of the smooth airfoil. It was found that the corrugation has both beneficial and detrimental effect on the aerodynamic performance. When the flow breaks from the corrugations, it immediately reattaches to the top surface and becomes caught in the valleys, delaying the separation of the flow. The corrugated skin delays the flow separation by 3°. At one hand it improves the stall angle. On the other hand, it somewhat reduces the lift coefficient at lower angle of attack and a rise in the drag coefficient is noticed. Although the maximum lift coefficient is increased by more than 19%, there is a reduction in maximum lift-to-drag ratio in the order of 20%. Hence the corrugation profile must be optimized to have the desired aerodynamic characteristics whereas minimizing the possible negative effect.

References

[1] Yuying Xia, Onur Bilgen and Michael I Friswel The effect of corrugated skins on aerodynamic performance, Journal of Intelligent Material Systems and Structures, 2014, Vol. 25(7) 786–794.

[2] CAMPANILE, L.F. and SACHAU, D. Belt-rib concept: a structronic approach to variable camber, J of Int Mat Sys and Struct, 2000, 11, (3), pp 215-224.

[3] KUDVA, J.N., Overview of the DARPA smart wing project, J of Int Mat Sys and Struct, 2004, 15, (4), pp 261-267.

[4] Rees CJC (1975a) Aerodynamic properties of an insect wing section and a smooth aerofoil. Nature 258(5531): 141–142.

[5] OKAMOTO, M., YASUDA, K. and AZUMA, A. Aerodynamic characteristics of the wings and body of a dragonfly, J of Experi Biology, 1996, 199, pp 281294.

[6] TAMAI, M., WANG, Z., RAJAGOPALAN, G., HU, H. and HE, G. Aerodynamic performance of a corrugated dragonfly airfoil compared with smooth airfoils at low Reynolds numbers, 45th AIAA Aerospace Sciences Meeting and Exhibition, 2007, Reno, NV, US

[7] Thill, C., Etches, J. A., Bond, I. P., Potter, K. D. and Weaver, P. (2007), "Corrugated composite structures for aircraft morphing skin applications", 18th International Conference of Adaptive Structures and Technologies, Ottawa, Ontario, Canada.

[8] Thill, C., Etches, J., Bond, I., Potter, K. and Weaver, P. (2008), "Morphing skins", The Aeronautical Journal, vol. 112, pp. 117-139.

[9] Yokozeki, T., Takeda, S., Ogasawara, T. and Ishikawa, T. (2006), "Mechanical properties of corrugated composites for candidate materials of flexible wing structures", Composites Part A: Applied Science and Manufacturing, vol. 37, no. 10, pp. 1578-1586.Rees CJC (1975a) Aerodynamic properties of an insect wing section and a smooth aerofoil. Nature 258(5531): 141–142.

[10] WHITEHEAD, D.S., Kodz, M. and Hield, P.M. Reduction of drag by corrugating trailing edges, Cambridge University, Engineering Department, (Technical Report) CUED/A-Turbo, 1982.Rees CJC (1975a) Aerodynamic properties of an insect wing section and a smooth aerofoil. Nature 258(5531): 141–142.

[11] C. Thill, J. D. Downsborough, S. J. Lai, I. P. Bond and D. P. Jones Aerodynamic study of corrugated skins for morphing wing applications, THE AERONAUTICAL JOURNAL, APRIL 2010 VOLUME 114 NO 1154.Rees CJC (1975a) Aerodynamic properties of an insect wing section and a smooth aerofoil. Nature 258(5531): 141–142.

[12] Hu, H., Tamai, M., "Bioinspired Corrugated Airfoil at Low Reynolds Numbers," Journal of Aircraft, Vol. 45, No. 6, 2008, pp. 2068-2077. Doi 10.2514/1.37173.

[13] Murphy, J. T., and Hu, H., "An Experimental Study of a Bio-Inspired Corrugated Airfoil for Micro Air Vehicle Applications," Experiments in Fluids, Vol. 49, No. 2, 2010, pp. 531–546.

[14] Levy, D.-E., and Seifert, A., "Simplified Dragonfly Airfoil Aerodynamics at Reynolds Numbers Below 8000," Physics of Fluids, Vol. 21, No. 7, 2009, p. 071901.

[15] T. H. New, ∗ Y. X. Chan,† and G. C. Koh†, M. C. Hoang‡, Shengxian Shi§ Effects of Corrugated Aerofoil Surface Features on Flow-Separation Control, AIAA JOURNAL Vol. 52, No. 1, January 2014.

[16] Zaeem Shabbir, Hassan R. Shah, Asif Mansoor, Syed M. Tayyab, Anwar Ahmed Effects of Varying Peak Shape on Aerodynamic Performance of a Corrugated Airfoil, presented at AIAA Scitech 2020 Forum, 6-10 January 2020, Orlando FL.

[17] Hu, H., Tamai, M., Marshall, J. and Plumb, R.A., 2008. Atmosphere, ocean and climate dynamics.

[18] Launder, B.E., 2015. First steps in modelling turbulence and its origins: a commentary on Reynolds (1895)'On the dynamical theory of incompressible viscous fluids and the determination of the criterion'. Philosophical Transactions of the Royal Society A: Mathematical, Physical and Engineering Sciences, 373(2039), p.20140231.

[19] Verhoff, A., Stookesberry, D. and Agrawal, S., 1992. Farfield computational boundary conditions for twodimensional external flow problems. AIAA journal, 30(11), pp.2585-2594.

NOMENCLATURE

c : chord length, mm
ρ : density, m^3
μ : absolute viscosity, kg/ms
τ_w : shear stress, N/m^2
α : angle of attack, deg
AoA : angle of attack, deg
C_{d0} : zero lift drag coefficient
C_d : drag coefficient
C_l : lift coefficient